Investigating the effects of cerebrospinal fluid removal on cerebral blood flow and oxidative metabolism in infants with post-hemorrhagic ventricular dilatation

Peter J. McLachlan[1], Jessica Kishimoto[1], Mamadou Diop[2], Daniel Milej[2], David S.C. Lee[3], Sandrine de Ribaupierre[4] and Keith St Lawrence[2]

BACKGROUND: Post-hemorrhagic ventricular dilatation (PHVD) is predictive of mortality and morbidity among very-low-birth-weight preterm infants. Impaired cerebral blood flow (CBF) due to elevated intracranial pressure (ICP) is believed to be a contributing factor.

METHODS: A hyperspectral near-infrared spectroscopy (NIRS) method of measuring CBF and the cerebral metabolic rate of oxygen ($CMRO_2$) was used to investigate perfusion and metabolism changes in patients receiving a ventricular tap (VT) based on clinical management. To improve measurement accuracy, the spectral analysis was modified to account for compression of the cortical mantle caused by PHVD and the possible presence of blood breakdown products.

RESULTS: From nine patients (27 VTs), a significant CBF increase was measured (15.6%) following VT (14.6 ± 4.2 to 16.9 ± 6.6 ml/100 g/min), but with no corresponding change in $CMRO_2$ (1.02 ± 0.41 ml O_2/100 g/min). Post-VT CBF was in good agreement with a control group of 13 patients with patent ductus arteriosus but no major cerebral pathology (16.5 ± 7.7 ml/100 g/min), whereas tissue oxygen saturation (StO_2) was significantly lower ($58.9 \pm 12.1\%$ vs. $70.5 \pm 9.1\%$ for controls).

CONCLUSION: CBF was impeded in PHVD infants requiring a clinical intervention, but the effect is not large enough to alter $CMRO_2$.

Despite advances in neonatal care and improved survival among premature infants, intraventricular hemorrhage (IVH) remains a persistent problem (12,000/year in the United States (1–3)). The extent of IVH, graded I–IV by Papile classification (4), is based on cranial ultrasound (US) and is highly predictive of the severity of symptoms, comorbidities, and mortality (5). Grade I, the mildest form, is a bleed confined to the germinal matrix; grade II describes a larger intraventricular bleed; grade III is reached when the bleeding leads to a distention of the ventricles; and grade IV is defined by periventricular hemorrhagic infarction. The prognosis is further worsened by the development of post-hemorrhagic ventricular dilatation (PHVD), which refers to the accumulation of cerebrospinal fluid (CSF) produced in the ventricles. Although mild ventriculomegaly typically resolves spontaneously, up to 80% of infants with grade IV and 50% with grade III will develop PHVD. According to the National Institute of Neurological Disorders and Stroke, PHVD is one of the most common sources of developmental disability in children (6–9).

The definitive treatment of PHVD is the placement of a ventriculo-peritoneal shunt to divert CSF from the brain to the peritoneal cavity (1). However, shunt placement is often delayed by several weeks to allow the blood clot to resolve and CSF protein levels to decrease. During this delay, intermediate interventions, such as repeated lumbar punctures or ventricular taps (VTs), are undertaken to avoid elevated intracranial pressure (ICP). Increased ICP compresses the cerebral mantle (the brain around the ventricles) and leads to brain damage in part by compromised cerebral energy metabolism resulting from impaired cerebral blood flow (CBF) (10). However, the timings of such interventions are subjective, typically based on a combination of clinical signs of elevated ICP: apnea, bradycardia, a rapid increase in head circumference (HC), and ventricle size as assessed by US, and a full tense fontanelle (5). Furthermore, these interventions carry a risk of hemorrhage and infection, and should only be conducted when absolutely necessary. Given these issues, there is a need for more sensitive techniques to guide PHVD management.

There is growing evidence of cerebral hemodynamic and metabolic disarrangement before the manifestation of clinical signs of elevated ICP, including suppressed background patterns detected by amplitude-integrated electroencephalography (aEEG) (3). There is also evidence that interventions to reduce elevated ICP improve cerebral perfusion, as indicated by restoration of a continuous aEEG pattern (11), increased cerebral blood flow velocity (12), and changes in cerebral oxygenation as measured by near-infrared

---

spectroscopy (NIRS) (13,14). These studies suggest that a means of assessing CBF and/or cerebral energy metabolism could help guide treatment decisions. NIRS is an obvious choice given that measurements can be collected at the bedside, the technology is extremely safe, and it has the capabilities to measure CBF and the cerebral metabolic rate of oxygen consumption (CMRO$_2$) (15–18).

The use of NIRS for neuro-monitoring preterm infants with PHVD presents some unique challenges, notably the reduction in cerebral mantle thickness (CMT) to 1 cm or less. NIRS data sets are typically acquired with a source-detector separation (SDS) around 3 cm to minimize the effects of light absorption in extra-cerebral tissues (19). This SDS could result in erroneous tissue oxygen saturation (StO$_2$) measurements given that light penetration depth, which is proportional to square root of the SDS (20), could be greater than the mantle thickness. In addition, the presence of blood breakdown products (BBPs) in the ventricles and surrounding tissue, in the case of grade IV IVH, could contaminate the NIRS signal. This could reduce the accuracy, given that most NIRS systems only acquire measurements at a few discrete wavelengths and assume that changes in light absorption are predominately related to oxy- and deoxy-hemoglobin concentrations ([HbO$_2$] and [Hb], respectively).

To address these challenges, we have developed a hyperspectral NIRS approach that accounts for cerebral thinning using a solution to the diffusion approximation based on a finite slab geometry, rather than the standard semi-infinite geometry (20), using CMT measurements from US images. In addition, the absorption spectra of BBPs were measured from CSF samples and incorporated into the data analysis algorithm. Monte Carlo simulations were conducted to assess the magnitude of error in StO$_2$ made without these steps. The developed NIRS approach was used to investigate changes in CBF, StO$_2$, and CMRO$_2$ in PHVD patients selected to undergo a VT based on clinical assessment. The measurements were compared with values from a control group to assess the overall effects of PHVD (15). Given the association of clinical signs such as apnea and bradycardia with elevated ICP, it was hypothesized that the tapping procedure would lead to an increase in CBF. The effects on CMRO$_2$ were less clear considering that lower CBF can be compensated for by an increase in the oxygen extraction fraction (OEF) (21).

METHODS

Patient Population
Following informed parental consent, 57 patients were enrolled in the study based on a diagnosis of IVH by routine cranial US. The severity of IVH was graded based on the Papile scale (4). Of 57 patients, 9 with PHVD required VTs based on clinical evidence (apnea, bradycardia, full fontanelles), and increased ventricle size as measured by US. Decisions on when to intervene were based on current clinical practice. The study protocol was approved by the Research Ethics Board of Western University (London, Ontario, Canada).

NIRS data from a previous study involving preterm neonates (<30 weeks gestational age) diagnosed with patent ductus arteriosus (15) were used as controls. These patients were selected to represent normal head spectra, as none of them had a diagnosis of moderate or severe IVH or any major congenital cerebral malformation. Data acquisition was performed with the same NIRS system used with the PHVD patients.

Study Design
After the decision to perform a VT was made, two NIRS data sets were acquired, one 5–10 min before and the other 10–60 min after the VT. The range was greater for the post-tap acquisitions, as it was delayed in neonates requiring resuscitation. NIRS data were acquired from the fronto-parietal cortex by probes placed on the scalp and held in place by a custom-built holder strapped to the head. The dynamic contrast-enhanced (DCE) NIRS protocol consisted of collecting spectra every 200 ms for a duration of 80 s, with indocyanine green (ICG) (0.1 mg/kg at a concentration of 0.5 mg/ml sterile water, BCD Pharma, Mississauga, Ontario, Canada) injected via a venous catheter at 10 s. The time-varying arterial ICG concentration was recorded simultaneously by a dye densitometer (DDG-2001, Nihon Kohden, Tokyo, Japan) attached to a foot.

Mean arterial blood pressure (MABP), arterial oxygen saturation (SaO2), heart rate (HR), transcutaneous partial pressure of carbon dioxide (TcPCO2), and HC were recorded before and after VT. Other recorded clinical measures included the mode of ventilation and total hemoglobin concentration, which was used to calibrate the arterial ICG concentration curve. The ventricular index was measured retrospectively from cranial US acquired closest to the first VT, as many centers use the 97th percentile + 4 mm of this measurement as an indicator to intervene (1). The CMT was measured from a coronal US image taken through the anterior fontanelle at the level of the foramen of Monro. The CMT was calculated as the average of two distances measured from the ventricular border to the skull, lateral and superior to the ventricles on the side of NIRS probes.

Spectral analysis was conducted on 2-ml CSF samples collected during the VT. The absorption spectrum was determined by spectrophotometry (Beckman DU-640, Beckman Coulter, Pasadena, CA, USA) using distilled water as a reference. The mean absorption spectrum of all samples was incorporated into the chromophore quantification fitting procedure (see Data Processing). For simulation purposes, CSF samples were divided into two groups based on color (yellow and red). Average absorption values for each color were included in Monte Carlo simulations performed to assess the influence of ventricular CSF on StO$_2$ measurements (see Error Analysis). In addition, the scattering properties of CSF were assessed by measuring the distribution of times of flight of photons (DTOFs) of transmitted light (760 nm) by time-resolved NIRS (22). DTOFs were measured for two samples (one yellow, one red), as well as a water reference, by placing each sample in a 2-cm-long polymer cuvette. Three-hundred DTOFs were collected and characterized by calculating the mean time of flight, $<t>$, and the full width at half maximum (FWHM). As light scattering in pure water is relatively small (23,24), these parameters were used to assess potential increases in scattering in the CSF samples.

Instrumentation
NIRS data were acquired with an in-house-built, broadband NIRS system (15). Light was generated by a 20-W halogen bulb (Ocean Optics HL-2000-HP, Dunedin, FL, USA) filtered from 600 to 1,000 nm and delivered to the head by a 2-m fiber-optic bundle (3.5 mm diameter, 0.55 numerical aperture). Another bundle with the same properties was used to collect reflected light and deliver it to the spectrometer (range from 680 to 980 nm, resolution = 0.38 nm/pixel; Sciencetech, London, Ontario, Canada). The spectrometer was coupled to a Peltier-cooled charge-coupled device camera (1024 × 124 matrix; Wright Instruments, Enfield, UK), which was operated as an array detector.

Data Processing

Quantifying chromophore concentrations. Photon flux through the head can be modeled using solutions to the diffusion approximation for specific geometries. The reflected flux is characterized in terms of an absorption coefficient, μ_a, and a reduced scattering coefficient, μ_s' (20). The most commonly used solution is for a semi-infinite medium, which is acceptable for infants as signal contamination from extra-cerebral tissues is small at SDS values of 3 cm and greater (25). The adaptation of this approach to spectral analysis has been described previously (26,27). With this approach, the wavelength dependency of μ_s' is modeled as follows (28):

$$\mu_s'(\lambda) = A \left(\frac{\lambda}{800} \right)^{-\alpha} \tag{1}$$

where A is the value of μ_s' at 800 nm. The μ_a is defined in terms of the main endogenous chromophores in tissue:

$$\mu_a(\lambda) = [HbO_2] \cdot \varepsilon_{HbO_2}(\lambda) + [Hb] \cdot \varepsilon_{Hb}(\lambda) + WF \cdot \varepsilon_{H_2O}(\lambda) \tag{2}$$

where $\varepsilon_i(\lambda)$ represents the extinction coefficient of the ith chromophore and WF is the tissue water fraction. For DCE NIRS, equation (2) can be expanded to include $\varepsilon(\lambda)$ for ICG.

Two modifications were made to the model for the analysis of spectra from PHVD patients. First, the solution to the diffusion approximation was based on a slab geometry representing the cortical mantle. This solution is composed of an infinite series of terms representing photon flux from virtual sources of increasing distances, both positive and negative, from the true source (20). It was determined that including the first five terms was sufficient to provide convergence. The second modification was to add another chromophore to μ_a to account for possible light absorption from BBPs:

$$\mu_a(\lambda) = [HbO_2] \cdot \varepsilon_{HbO_2}(\lambda) + \cdot \varepsilon_{Hb}(\lambda) + WF \cdot \varepsilon_{H_2O}(\lambda) + k \cdot \mu_{a,BBP}(\lambda) \tag{3}$$

where $\mu_{a,BBP}$ is the mean spectrum across all CSF samples. The scaling factor, k, is included, as the concentration of breakdown products in the samples was not measured.

Spectral analysis began by applying a de-noising algorithm that consisted of transforming the noise from Poisson to Gaussian, removing the latter by wavelet de-noising, and applying an inverse transformation to obtain noise-free spectra (26). Chromophore concentrations were determined by fitting the model to the first and second derivatives of reflectance data. First, WF was determined by fitting the second derivative spectrum to the water feature between 815 and 840 nm. Using WF, [Hb] was determined by fitting the second derivative spectrum to the 760-nm Hb feature over the range from 690 to 775 nm. Last, [HbO_2], k, A, and α were determined by fitting the first derivative spectrum from 690 to 840 nm with WF and [Hb] fixed. Fitting was performed using a constrained optimization routine (MATLAB script *fminsearchbnd*) with upper and lower boundaries set to published values. [HbO_2] and [Hb] were determined from the mean spectrum acquired before ICG was injected and used to calculate StO_2:

$$StO_2 = \frac{[HbO_2]}{[Hb] + [HbO_2]} \tag{4}$$

Quantifying CBF and CMRO₂. CBF was determined from the time-varying ICG concentration in brain measured by NIRS, $C_b(t)$, and the corresponding arterial concentration curve measured by dye densitometry, $C_a(t)$. The two curves are related to CBF as follows:

$$C_b(t) = C_a(t) * CBF \cdot R(t) \tag{5}$$

where * indicates the convolution operator and $R(t)$ represents the amount of ICG in brain following an idealized bolus injection of unit concentration (29). The flow-scaled $R(t)$ was determined by

deconvolution (21) and its initial height is equal to CBF as $R(t=0) = 1$.

CMRO_2 was calculated based on the Fick principle:

$$CMRO_2 = \frac{CBF \cdot K}{f_v} \cdot [tHb] \cdot (SaO_2 - StO_2) \tag{6}$$

where K is the oxygen-carrying capacity of hemoglobin (1.39 ml of O_2/g of Hb) and f_v is the venous cerebral blood volume fraction, assumed to be equal to 0.75 (22).

Error Analysis

Simulated StO_2 values were generated by Monte Carlo simulations to test for errors caused by reduced CMT and the presence of BBPs in the ventricles. Simulations were conducted for 730 and 810 nm, and SDS values of 3 and 4 cm, similar to commercial NIRS methods (30). Light propagation was performed using the CUDAMCML (31,32) software package in a two-layer (brain, ventricle) simulation volume. Photon reflectance data were generated as the thickness of the top layer varied from 10 to 30 mm. The lower limit of 10 mm was set based on the minimum CMT measured in patients. For all simulations, μ_a of brain was calculated from equation (2) with a total hemoglobin concentration (tHb) of 15 g/dl, [Hb] and [HbO_2] values corresponding to StO_2 = 70%, a water fraction of 85%, and μ_s' of 1 mm^{-1} (33). For the ventricle layer, $\mu_s' = 0.01$ mm^{-1} (34) and μ_a varied over three conditions representing red, yellow, and clear CSF (0.066, 0.0096, 0.0021 mm^{-1}, respectively, at 730 nm and 0.059, 0.0075, 0.0022 mm^{-1}, respectively, at 810 nm). The μ_a values for red and yellow CSF were set to the values measured by spectrophotometry and μ_a for clear CSF was set to the literature values for water (24).

StO_2 was calculated using the spatially resolved approach (35). Taking the log of the reflected light intensity, $R(r)$, scaled by the square of the SDS, r, results in the following:

$$\ln\left[R(r) \cdot r^2\right] = r \cdot Slope + Intercept \tag{7}$$

where "Slope" is the slope of the reflectance loss between two r values and is given as follows:

$$Slope = \frac{\mu_a}{3(\mu_a + \mu_s')} \cong \frac{\mu_a}{3\mu_s'} \tag{8}$$

If μ_s' is assumed, typically set to 1 mm^{-1} (25,34), then μ_a can be computed for the measured slope. [Hb] and [HbO_2] can be determined from the μ_a values measured at 730 and 810 nm (30).

Statistical Analysis

Nonparametric tests were used to assess statistical significance. Mann–Whitney U tests were performed to assess the difference before and after VT for CBF, StO_2, CMRO_2, as well as for SaO_2, HR, BP, and tscCO_2. Wilcoxon signed-rank tests were used to determine significance between pre-VT PHVD data and the control group. Statistical significance was based on a P-value of < 0.05. Data are presented as mean ± standard error (SE) unless stated otherwise.

RESULTS

Patients Studied

NIRS data were acquired from 10 patients requiring multiple VTs (27 in total). Data from three patients (7 taps) were excluded because of sizable artifacts in the arterial ICG curves caused by excessive foot motion. One additional set was removed because of the poor quality of the NIRS spectra, which was attributed to ambient light contamination. The remaining 20 taps from 9 patients were analyzed and the clinical measures are summarized in **Table 1**. Included in the table are the relevant clinical data from the control group (15).

Table 1. Clinical parameters for the PHVD patients who required interventional ventricle tap

	PHVD patients	Controls
Gestational age at birth (weeks ± SD, (range))	26.9 ± 1.8 (24 6/7–29)	27 (24 3/7–35 5/7)
Birth weight (g ± SD, (range))	1,011 ± 206 (750–1,280)	1,035 (630–2,135)
Sex	M = 6, F = 3	M = 8, F = 5
Apgar 1 min (mean, (range))	2.9 (1–8)	4 (2–8)
Number of VT required (mean, (range))	2.4 (1–5)	0
Age at first VT (days ± SD (range))	17.7 ± 8.7 (7–35)	NA
EVD (N)	2	NA
VP shunt (N)	7	NA
Neonatal death (N)	1	0
Cortical mantle thickness (cm)	1.23 ± 0.3 (0.96–1.74)	NA
IVH (N)		
Bilateral III	4	0
Grade IV(R)/III(L)	3	0
Grade IV(L)/III(R)	1	0
Bilateral IV	1	0

EVD, extraventricular drain; IVH, intraventricular hemorrhage; NA, not available; SD, standard deviation; VP, ventriculoperitoneal shunt.

CSF Samples

The CSF samples fell into one of two categories based on color (dark red or yellow), which was not unexpected given that the BBPs are oxyhemoglobin, methemoglobin (dark brown), and bilirubin (straw colored) (36). The mean absorption spectra for the two categories, along with the mean spectrum across all samples, are illustrated in **Figure 1**. These spectra all displayed decreasing absorption with increasing wavelength. Given that the spectra of oxyhemoglobin and methemoglobin increase from 700 to 1,000 nm (37), the predominant chromophore was likely to be bilirubin, which also exhibits an inverse wavelength dependency (38).

The FWHM of the DTOFs for yellow and red CSF samples (560 and 585 ps, respectively) were very similar to that of water (559 ps). Similarly, $<t>$ values for the yellow (466 ps) and red (470 ps) samples were only 2 and 9% greater than those of water (462 ps). The close agreement between the samples indicates that scattering had negligible effects.

Absorption Spectra

Figure 2a presents measured pre-tap spectrum from one patient with a CMT = 11 mm and diagnosed with bilateral grade III IVH. For comparison, the figure includes the mean absorption spectrum from the control group. **Figure 2b** presents theoretical absorption spectra generated from the diffusion approximation for a semi-infinite medium and
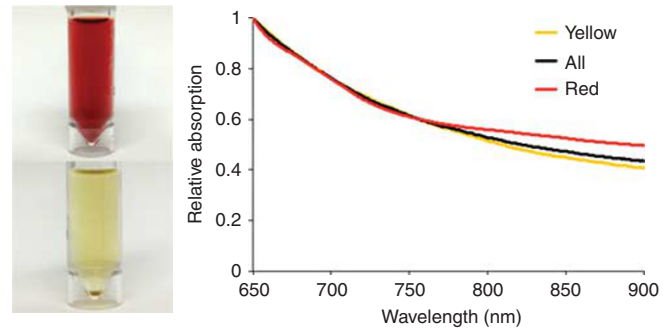

Figure 1. Representative red and yellow CSF samples (left) and mean absorption spectra for the red and yellow groupings (four and nine samples, respectively) along with the mean of all samples (right). Spectra for individual CSF samples were normalized to their value at 650 nm to account for absorption variations due to concentration differences. CSF, cerebrospinal fluid.

a 11-mm-thick slab. Spectra were generated with identical tissue properties (StO$_2$ = 0.7, $\mu_s' = 1$ mm^{-1}, water fraction = 0.85, and tHb = 150 g/l) to illustrate the effects of a finite turbid layer on the reflectance spectrum.

Average first and second derivative spectra, before and after VT, are shown in **Figure 3**. For reference, each graph includes the corresponding spectrum for the control group. In general, the pre- and post-tap second derivative spectra were very similar to the control spectrum, specifically at the 760-nm Hb feature and water feature between 815 and 840 nm. In contrast, there was a noticeable downward shift in the first derivative spectra from the PHVD patients; however, the differences between pre- and post-tap spectra were considerably smaller.

Pre- and Post-VT Measures

Pre- and post-tissue ICG concentration curves from one infant are shown in **Figure 4**. In this example, CBF increased by 14.7% from 13.4 to 15.4 ml/100 g/min. **Table 2** provides the average pre- and post-VT values of CBF and CMRO$_2$ along with the fitting parameters from the spectral analysis. There was a significant increase in CBF following VT, along with a significant increase in [HbO$_2$]. Corresponding differences in [Hb], StO$_2$, OEF, and CMRO$_2$ were small and did not reach significance. Similarly, there were no significant changes in the scattering parameters, although the difference in α pre- and post-VT was close to significant. Among the clinical data (**Table 1**), only HC showed a significant change after VT with a reduction of about 1 cm.

Comparison between PHVD patients and controls

Average values of the fitting parameters, CBF, OEF, and CMRO$_2$ from the PHVD group (pre-VT) and controls are given in **Table 3**. A significant decrease in StO$_2$ and a corresponding increase in OEF were found for PHVD patients. However, there was no significant difference with respect to CBF and CMRO$_2$. The wavelength-dependent scattering variable α was significantly higher in the PHVD group.
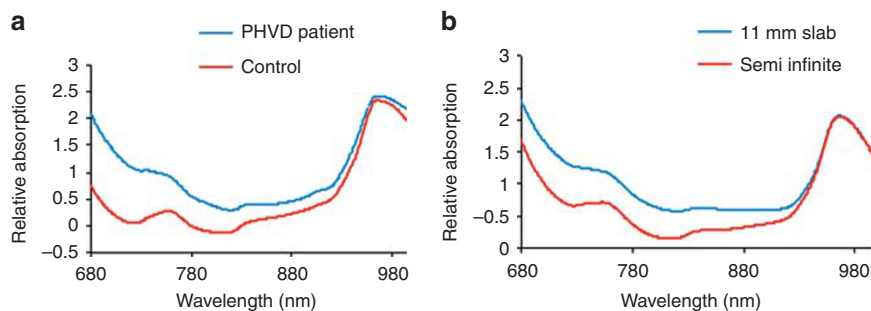
Figure 2. Absorption spectra. (**a**) Measured head spectra from the control group (red) and a PHVD patient with CMT = 11 mm. (**b**) Simulated absorption spectra based on the principle chromophores (water and hemoglobin) in the brain using a semi-infinite (red) and 11-mm slab model (blue). CMT, cerebral mantle thickness; PHVD, post-hemorrhagic ventricular dilatation.
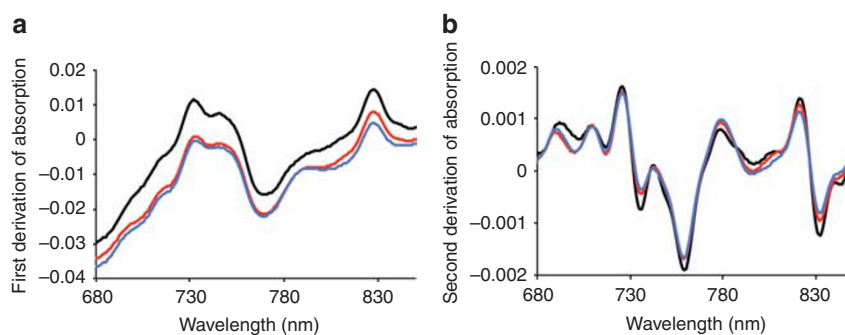

Figure 3. Derivative spectra. Average first (**a**) and second (**b**) derivative spectra before (blue) and after (red) ventricle tap. Each graph also includes the corresponding spectrum from the control group (black). Each patient's spectrum was averaged over 50 repetitions acquired in the 10-s period before ICG injection.
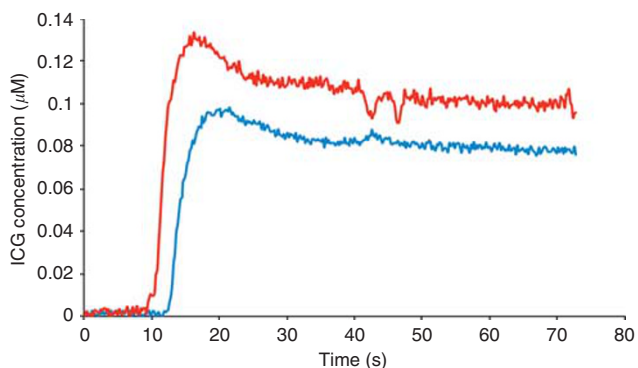

Figure 4. ICG concentration curves measured by DCE NIRS before VT (blue) and after (red) VT from a patient with bilateral grade III IVH. DCE, dynamic contrast-enhanced; IVH, intraventricular hemorrhage; NIRS, near-infrared spectroscopy; VT, ventricle tap.

Table 2. Mean NIRS and clinical parameters before and after VT

Parameter	Before VT	After VT	Change (%)	Significance (P-value)
CBF (ml/100 g/min)	14.6 ± 1.0	16.9 ± 1.5	15.6	**0.006**
[Hb] (g/dl)	15.2 ± 1.0	16.4 ± 1.4	10.2	0.50
[HbO$_2$] (g/dl)	26.3 ± 4.6	30.0 ± 4.4	11.9	**0.035**
tHb (g/dl)	41.5 ± 4.8	46.4 ± 4.8	12.0	0.075
SaO$_2$ (%)	92.7 ± 0.8	91.8 ± 0.8	− 1.0	0.13
StO$_2$ (%)	58.9 ± 2.7	61.0 ± 2.8	3.1	0.35
CMRO$_2$ (ml O$_2$/100 g/min)	1.00 ± 0.08	1.04 ± 0.10	4.9	0.33
OEF	0.36 ± 0.03	0.34 ± 0.03	− 7.1	0.078
A (mm^{-1})	0.37 ± 0.04	0.34 ± 0.03	− 7.3	0.22
α	3.9 ± 0.32	4.4 ± 0.30	16	0.055
HC (cm)	28.4 ± 0.1	27.5 ± 0.1	− 3.1	<**0.001**
HR (bpm)	157 ± 0.4	159 ± 0.5	1.5	0.19
MABP	51.8 ± 0.6	48.9 ± 0.5	− 5.7	0.21
TcsCO$_2$	54.4 ± 0.8	56.5 ± 0.7	3.9	0.37

CBF, cerebral blood flow; CMRO$_2$, cerebral metabolic rate of oxygen; HC, head circumference; HR, heart rate; MABP, mean arterial blood pressure; OEF, oxygen extraction fraction; NIRS, near-infrared spectroscopy; PHVD, post-hemorrhagic ventricular dilatation; tHb, total hemoglobin; VT, ventricle tap.
Values were averaged over 20 data sets.
Significant values are indicated in bold.

Error Analysis

StO$_2$ derived from simulated data for the two-layer model (brain and ventricle CSF) showed increasing underestimation, as the CMT was reduced to <15 mm. This underestimation, based on a nonscattering CSF layer, did not change when the μ_a values for red or yellow CSF were used instead of the values for water (**Figure 5**).

Table 3. Mean NIRS parameters from the PHVD patients and controls

Parameter	Controls	PHVD	Change (%)	Significance (*P*-value)
CBF (ml/100 g/min)	16.5 ± 2.1	14.6 ± 1.0	-11.8	0.32
[Hb] (g/dl)	12.9 ± 0.9	15.2 ± 1.0	17.9	0.051
[HbO$_2$]	32.0 ± 4.2	26.3 ± 4.6	-17.9	**0.043**
tHb (g/dl)	44.9 ± 4.0	41.5 ± 4.8	-7.7	0.20
StO$_2$ (%)	70.5 ± 2.4	58.9 ± 2.7	-16.4	**0.004**
CMRO$_2$ (ml O$_2$/100 g/min)	0.90 ± 0.14	1.00 ± 0.08	10.5	0.084
OEF	0.25 ± 0.02	0.36 ± 0.03	43.3	**0.007**
A (mm^{-1})	0.35 ± 0.03	0.37 ± 0.04	9.6	0.51
α	2.7 ± 0.1	3.9 ± 0.32	45.5	**0.025**

CBF, cerebral blood flow; CMRO$_2$, cerebral metabolic rate of oxygen; OEF, oxygen extraction fraction; NIRS, near-infrared spectroscopy; PHVD, post-hemorrhagic ventricular dilatation; tHb, total hemoglobin.
Significant values are indicated in bold.
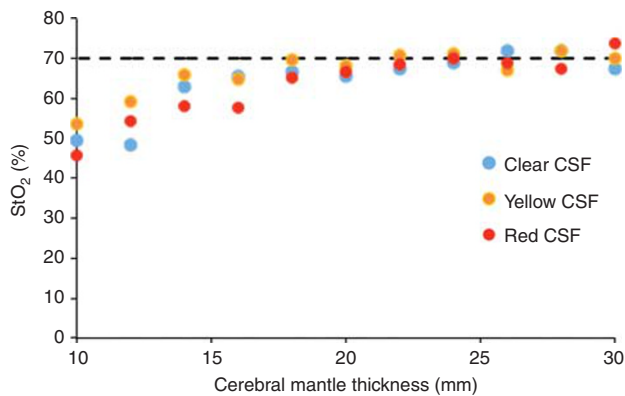
Figure 5. StO$_2$ vs. cerebral mantle thickness for CSF with μ_a values that reflected water (clear CSF) or values for red and yellow samples. CSF, CSF, cerebrospinal fluid.

DISCUSSION

The aims of this study were to develop an analysis method to address the unique challenges of applying NIRS to PHVD patients and to use the method to investigate possible improvements in CBF and CMRO$_2$ due to alleviation of elevated ICP after a VT. Regarding the first aim, there was clear evidence from cranial US that the thickness of the brain was considerably reduced in these patients. The mean CMT from nine patients was 1.2 ± 0.1 cm with a range from 1 to 1.7 cm, whereas the CMT in a normal preterm brain would typically be > 2 cm. To investigate how compressing the mantle affects the accuracy of NIRS, Monte Carlo simulations were performed using a two-layer model to represent the cortical mantle and the ventricular space. Reflectance data were generated for SDS of 3 and 4 cm, which are recommended to minimize signal contamination from superficial tissue (35), and used to estimate StO$_2$ by spatially

resolved NIRS. The simulations indicated that StO$_2$ was increasingly underestimated, as the CMT approaches 1 cm because of the loss of light into the ventricles, which is not accounted for when the brain is modeled as a semi-infinite medium (**Figure 5**). In this study, compression of the cortical mantle was accounted for by analyzing the measured spectra with a slab solution to the diffusion approximation. This approach takes advantage of the fact that the CMT can be estimated by readily available US images. Interestingly, the changes in the reflectance spectrum predicted by the slab model were similar to those observed experimentally (**Figure 2**).

A second consideration was the possibility of additional light absorption because of the presence of BBPs. To address this, absorption spectra from CSF samples were measured and incorporated into the fitting routine. Although there are differences between the spectra for red and yellow CSF samples, their overall shapes were similar (**Figure 1**) and, therefore, the mean spectrum of all samples was used in the fitting procedure. Using a mean spectrum could result in errors due to time-dependent variations in the relative contributions of BBPs. However, StO$_2$ was usually not influenced by including $\mu_{a,BBP}(\lambda)$ and the best-fit estimate of the scaling factor k was close to zero. In only two cases, both classified as grade IV IVH, did including this parameter influence the fitting: pre-VT StO$_2$ dropped from 74 to 49% in one case and from 65 to 60% in the other when $\mu_{a,BBP}$ was not included. In these cases, bleeding into the brain may have affected light absorption. The negligible contribution of $\mu_{a,BBP}(\lambda)$ for all other patients can be explained by the low scattering properties of CSF, as indicated by the TR-NIRS results. In these cases, the ventricles would act as a light 'sink' as the amount of back-scattered light in the ventricles would be insignificant. These findings are in agreement with the Monte Carlo results that showed similar StO$_2$ values across the range of CMTs regardless of whether $\mu_a(\lambda)$ of the CSF layer was set to values of water or those determined from CSF samples.

Regarding the clinical aim of this study, significant increases in CBF and [HbO$_2$] were found following VT, likely because of reduced ICP as suggested by the corresponding reduction in HC. However, this is a speculation, as ICP measurements were not acquired as part of this study. The CBF increase was in agreement with previous Doppler flow and NIRS oxygenation studies that reported increases in their respective measurements following similar interventions (13,14,39). Unlike previous studies that provided indirect measures of CBF, such as the oxygenation difference signal (HbO$_2$ − Hb), the use of DCE NIRS enabled CBF to be measured directly. The benefits were not only to confirm that CSF removal does improve CBF but also to show that the perfusion change was fairly modest with a mean increase of 15%. To put this in context, the same DCE NIR approach was used previously to show that CBF decreased by 20–30% in preterm infants administered the vasoconstrictor indomethacin as treatment for patent ductus arteriosus (15,21). Despite this reduction in CBF, CMRO$_2$ was not affected by indomethacin because of a

compensatory increase in OEF. In light of these previous findings, it is not surprising that no significant decompression-related change in $CMRO_2$ was found. Elevated OEF before VT would be expected to compensate for lower CBF. A trend toward a reduction in OEF after VT was observed, but it did not reach statistical significance. The lack of a metabolic effect is in line with Soul *et al.* (14) who reported no change in cerebral cytochrome oxidase. Unlike Norooz *et al.* (13), no significant change in StO_2 was observed with treatment, which could be related to differences in the type of treatment and timing of the measurements. The Norooz study used external ventricular drainage for decompression, and StO_2 was measured 24 h after the procedure. Another discrepancy was that the mean preintervention StO_2 (43%) was considerably lower than the value found in the current study (59%). This could be explained by patient selection differences, or a consequence of the sources of error discussed above.

Compared with controls, PVHD patients had significantly lower StO_2 and higher OEF. These changes suggest reduced oxygen delivery, although it is not clear why treatment-related improvements were not detected considering the agreement between post-VT CBF and mean CBF from controls (16.9 vs. 16.5 ml/100 g/min, respectively). A limitation is that StO_2 and OEF were only measured at single times, and it is conceivable that extending the monitoring could have detected further oxygenation changes. Alternately, StO_2 may still be underestimated in the PHVD group because of uncertainty in US measurements of the CMT, although these were made as close as possible to the NIRS probes to minimize errors. It is also possible that the slab solution to the diffusion approximation did not adequately model light propagation through the head. This solution assumes planar geometry and factors such as the curvature of the head and variations in CMT may lead to errors. Monte Carlo simulations incorporating segmented head models could be used to address these issues (25). Interestingly, it was also found that the parameter α was greater in PHVD patients, suggesting that compression of the cortical mantle altered the tissue scattering properties.

CONCLUSIONS

This study presents a hyperspectral NIRS method of measuring CBF and $CMRO_2$ in PHVD patients. Using a patient-specific analysis approach that incorporated US measurements of CMT, the NIRS results indicated that VT improved CBF but had no effect on $CMRO_2$, likely reflecting a compensatory increase in oxygen extraction. Compared with controls, PHVD was associated with significantly lower StO_2 and elevated OEF, which are indications of possible restricted oxygen delivery. These results suggest that NIRS could play a useful role in determining the impact of PHVD on patient health. Continuous monitoring achievable by incorporating diffuse correlation spectroscopy (15,40) would be beneficial to investigate longer-term perfusion and metabolic changes leading up to and following clinical interventions.

REFERENCES
1. Whitelaw A, Aquilina K. Management of posthaemorrhagic ventricular dilatation. Arch Dis Child Fetal Neonatal Ed 2012;97:F229–33.
2. Calisici E, Eras Z, Oncel MY, et al. Neurodevelopmental outcomes of premature infants with severe intraventricular hemorrhage. J Matern Fetal Neonatal Med 2014;7058:1–6.
3. Olischar M, Klebermass K, Kuhle S, et al. Progressive posthemorrhagic hydrocephalus leads to changes of amplitude-integrated EEG activity in preterm infants. Child's Nerv Syst 2004;20:41–5.
4. Papile LA, Burstein J, Burstein R, et al. Incidence and evolution of subependymal and intraventricular hemorrhage: a study of infants with birth weights less than 1,500 gm. J Pediatr 1978;92:529–34.
5. Whitelaw A. A different view: there is value in grading intraventricular hemorrhage. Acta Paediatr Int J Paediatr 2007;96:1257–8.
6. Adams-Chapman I, Hansen NI, Stoll BJ, Higgins R. Neurodevelopmental outcome of extremely low birth weight infants with posthemorrhagic hydrocephalus requiring shunt insertion. Pediatrics 2008;121:e1167–77.
7. Hill A. Ventricular dilation following intraventricular hemorrhage in the premature infant. Can J Neurol Sci 1983;10:81–5.
8. Guyer B, MacDorman MF, Martin JA, Peters KD, Strobino DM. Annual summary of vital statistics - 1997. Pediatrics 1998;102:1333–49.
9. Wilson-Costello D, Friedman H, Minich N, et al. Improved survival rates with increased neurodevelopmental disability for extremely low birth weight infants in the 1990s. Pediatrics 2005;115:997–1003.
10. Maertzdorf WJ, Vles JSH, Beuls E, et al. Intracranial pressure and cerebral blood flow velocity in preterm infants with posthaemorrhagic ventricular dilatation. Arch Dis Child Fetal Neonatal Ed 2002;87:F185–8.
11. Olischar M, Klebermass K, Hengl B, et al. Cerebrospinal fluid drainage in posthaemorrhagic ventricular dilatation leads to improvement in amplitude-integrated electroencephalographic activity. Acta Paediatr Int J Paediatr 2009;98:1002–9.
12. Hill A, Volpe JJ. Decrease in pulsatile flow in the anterior cerebral arteries in infantile hydrocephalus. Pediatrics 1982;69:4–7.
13. Norooz F, Urlesberger B, Giordano V, et al. Decompressing posthaemorrhagic ventricular dilatation significantly improves regional cerebral oxygen saturation in preterm infants. Acta Paediatr 2015;104:663–9.
14. Soul JS, Eichenwald E, Walter G, et al. CSF removal in infantile posthemorrhagic hydrocephalus results in significant improvement in cerebral hemodynamics. Pediatr Res 2004;55:872–6.
15. Diop M, Kishimoto J, Toronov V, et al. Development of a combined broadband near-infrared and diffusion correlation system for monitoring cerebral blood flow and oxidative metabolism in preterm infants. Biomed Opt Express 2015;6:3907–18.
16. Kissack CM, Weindling AM. Peripheral blood flow and oxygen extraction in the sick, newborn very low birth weight infant shortly after birth. Pediatr Res 2009;65:462–7.
17. Yoxall CW, Weindling AM. Measurement of cerebral oxygen consumption in the human neonate using near infrared spectroscopy: cerebral oxygen consumption increases with advancing gestational age. Pediatr Res 1998;44:283–90.
18. Elwell CE, Owen-Reece H, Cope M, et al. Measurement of adult cerebral haemodynamics using near infrared spectroscopy. Acta Neurochir Suppl 1993;59:74–80.

19. Demel A, Feilke K, Wolf M, et al. Correlation between skin, bone, and cerebrospinal fluid layer thickness and optical coefficients measured by multidistance frequency-domain near-infrared spectroscopy in term and preterm infants. J Biomed Opt 2014;19:17004.

20. Martelli F, Del Bianco S, Ismaeilli A, et al. Light Propagation Through Biological Tissue and Other Diffusive Media. Bellingham, WA: SPIE Press, 2010:57–79.

21. Arora R, Ridha M, Lee DSC, et al. Preservation of the metabolic rate of oxygen in preterm infants during indomethacin therapy for closure of the ductus arteriosus. Pediatr Res 2013;73:713–8.

22. Verdecchia K, Diop M, Lee T-Y, et al. Quantifying the cerebral metabolic rate of oxygen by combining diffuse correlation spectroscopy and time-resolved near-infrared spectroscopy. J Biomed Opt 2013;18:27007.

23. Buiteveld H, Haakvort JHM, Donze M. The optical properties of pure water. Proc SPIE 1994;12:174–83.

24. Smith CR, Baker SK. Optical properties of the clearest natural waters (200-800 nm). Appl Opt 1981;20:177–84.

25. Dehaes M, Grant PE, Sliva DD, et al. Assessment of the frequency-domain multi-distance method to evaluate the brain optical properties: Monte Carlo simulations from neonate to adult. Biomed Opt Express 2011;2:552–67.

26. Diop M, Wright E, Toronov V, et al. Improved light collection and wavelet de-noising enable quantification of cerebral blood flow and oxygen metabolism by a low-cost, off-the-shelf spectrometer. J Biomed Opt 2014;19:057007.

27. Yeganeh HZ, Toronov V, Elliott JT, et al. Broadband continuous-wave technique to measure baseline values and changes in the tissue chromophore concentrations. Biomed Opt Express 2012;3:2761–70.

28. Jacques SL. Optical properties of biological tissues: a review. Phys Med Biol 2013;58:R37–61.

29. Zierler KL. Equations for measuring blood flow by external monitoring of radioisotopes. Circ Res 1965;16:309–21.

30. Hyttel-Sorensen S, Hessel TW, la Cour A, et al. A comparison between two NIRS oximeters (INVOS, OxyPrem) using measurement on the arm of adults and head of infants after caesarean section. Biomed Opt Express 2014;5:3671.

31. Wang L, Jacques SL, Zheng L. MCML-Monte Carlo modeling of light transport in multi-layered tissues. Comput Methods Programs Biomed 1995;47:131–46.

32. Erik Alerstam SA-E. Monte Carlo Simulations of Light Transport in Tissue. University of Lund: Lund, Sweden, 2008:1–12.

33. Brigadoi S, Aljabar P, Kuklisova-Murgasova M, et al. A 4D neonatal head model for diffuse optical imaging of pre-term to term infants. Neuro-image 2014;100:385–94.

34. Okada E, Delpy DT. Near-infrared light propagation in an adult head model. II. Effect of superficial tissue thickness on the sensitivity of the near-infrared spectroscopy signal. Appl Opt 2003;42:2915–2.

35. Metz AJ, Biallas M, Jenny C, et al. The effect of basic assumptions on the tissue oxygen saturation value of near infrared spectroscopy. Adv Exp Med Biol 2013;765:169–75.

36. Barrows LJ, Hunter FT, Banker BQ. The nature and clinical significance of pigments in the cerebrospinal fluid. Brain 1955;78:59–80.

37. Lee J, El-Abaddi N, Duke A, et al. Noninvasive in vivo monitoring of methemoglobin formation and reduction with broadband diffuse optical spectroscopy. J Appl Physiol 2006;100:615–22.

38. Cope M The Application of Near Infrared Spectroscopy to Non Invasive Monitoring of Cerebral Oxygenation in the Newborn Infant. University College London: London, UK, 1991.

39. van Alfen-van der Velden AA, Hopman JC, Klaessens JH, et al. Cerebral hemodynamics and oxygenation after serial CSF drainage in infants with PHVD. Brain Dev 2007;29:623–9.

40. Durduran T, Yodh AG. Diffuse correlation spectroscopy for non-invasive, micro-vascular cerebral blood flow measurement. Neuroimage 2014;85: 51–63.